Chemical Engineering Science 275 (2023) 118718

Contents lists available at ScienceDirect

Chemical Engineering Science

journal homepage: www.elsevier.com/locate/ces

The charge regulation of surfactants on the rock surface in nanoconfinement: A reaction-coupling fluid density functional theory study

Jipeng Xu [a,1], Jin Cheng [a,1], Jie Yang [a], Haolan Tao [a], Sijie Wang [a], Wenjie Lv [b,*], Ke Ma [c,*], Cheng Lian [a,*], Honglai Liu [a]

[a] State Key Laboratory of Chemical Engineering, Shanghai Engineering Research Center of Hierarchical Nanomaterials, and School of Chemistry and Molecular Engineering, East China University of Science and Technology, Shanghai 200237, China
[b] National Engineering Research Center of Industrial Wastewater Detoxication and Resource Recovery, East China University of Science and Technology, Shanghai 200237, China
[c] Tianjin Key Laboratory for Photoelectric Materials and Devices, School of Materials Science and Engineering, Tianjin University of Technology, Tianjin 300384, China

HIGHLIGHTS

- Joint fluid DFT and surface reaction model could accurately predict surface charge density and ζ potential of rock.
- The pore size effect became negligible with the increasing surfactant concentration.
- The upper limit of charge regulation performance emerges as the surfactant concentration increases.
- The ζ potential exhibits less negative with the increasing surfactant concentration due to the electrostatic screening.
- The chain length effect is significant in cationic surfactants systems, while anionic surfactants' behavior is similar to simple salt.

ARTICLE INFO

Article history:
Received 12 January 2023
Received in revised form 27 March 2023
Accepted 2 April 2023
Available online 6 April 2023

Keywords:
Fluid density functional theory
Surface reaction model
Surfactant
Charge regulation
Silica pores

ABSTRACT

The surface charge density and ζ potential of rock play an essential role in chemical enhanced oil recovery (CEOR), but the electrochemical properties of rock surfaces are difficult to predict under different reservoir conditions. Therefore, a new method was proposed combining fluid density functional theory (fluid DFT) and the surface reaction model. The surface charge density and ζ potential of silica pores under different conditions were predicted, in which the effects of pH, pore size (d), surfactant chain length (N), surfactant type, and concentration on the charge regulation of silica pores were thoroughly investigated. The surface tends to be more negatively charged with increasing pH and surfactant concentration. Moreover, the pore size effect is not negligible in charge regulation, but there is a critical pore size (CPS) that decreases as the surfactant concentration and pH increase. The difference between anionic and cationic surfactants is also investigated, which display different behaviors under nanoconfinements. The anionic surfactants' behavior is similar to that of the simple salt. Furthermore, the ζ potential of silica pores increased as the surfactant concentration increased due to electrostatic screening, which is consistent with the results of molecular dynamics (MD) simulations and experiments.

1. Introduction

With the increasing demand for petroleum resources, it has become urgent to gradually improve the efficiency and economy of oil recovery. It is traditionally considered that the surface macroscopic properties of rock play a vital role in oil recovery, consisting of permeability, wettability, roughness, etc. For instance, the injection of low salinity water (Gandomkar and Rahimpour, 2015), gas (Gandomkar et al., 2022), and surfactant (Chowdhury et al., 2022; Kamal et al., 2017) could induce wettability alternation, helping boost oil production. However, most studies only focus on experimental phenomena in an open space, such as contact angle and interfacial tension, which is obviously different from real reservoir conditions, as the confined environment is neglected. It has been found that the fluids in nanoconfinement are induced to exhibit different properties compared with the bulk phase (Ritt

* Corresponding authors.
E-mail addresses: lvwj@ecust.edu.cn (W. Lv), kema@tjut.edu.cn (K. Ma), liancheng@ecust.edu.cn (C. Lian).
[1] These authors contributed equally.

https://doi.org/10.1016/j.ces.2023.118718
0009-2509/

et al., 2022; Nazari et al., 2020). Meanwhile, the interfacial electrochemical properties of rock surfaces, which are closely related to oil recovery, have not received enough attention (Ong et al., 2020; Nasralla et al., 2013). Having investigated how ionic strength and pH affected the adhesion behavior and wettability of crude oil on the mineral surface, Buckley et al. (Buckley et al., 1989) demonstrated that increasing pH may result in a more negative charge and ζ potential of the oil/water interface, and the expanding electric double layers due to the low saline brine could improve the oil recovery (Alroudhan et al., 2016). Gandomkar et al. (Amiri and Gandomkar, 2019) proposed that seawater injection led to a negative charge at the oil/rock interface so that the repulsion between rock and oil was increased, causing the oil to be displaced from the rock surface. Moreover, Nasr-El-Din (Alotaibi and Nasr-El-Din, 2011) and Jackson (Jackson et al., 2016) proposed that the improvement in oil recovery was closely correlated to the ζ potential and surface charge. Therefore, it is important to develop a deep understanding of fluid and rock properties, especially charge regulation under confined conditions, including the two representative descriptors, surface charge density and ζ potential of the rock surface, which is beneficial to deep insights into chemical enhanced oil recovery (CEOR).

Currently, multiscale methods have been carried out to investigate the effect of surfactants or inorganic salts on rock surface properties, consisting of quantum density functional theory (QDFT) (Cao et al., 2021; El Haouti et al., 2019) and molecular dynamic (MD) simulation (Aminian and ZareNezhad, 2019; Brkljača et al., 2018; Koleini et al., 2018; Xu et al., 2021). Compared to MD simulation, QDFT requires more time and economic costs, and the simulation results are usually obtained in a vacuum, with a significant difference from actual conditions. In our previous work, QDFT was employed to reveal the interaction type and strength among oil components, in which the number of atoms does not exceed 300 (Xu et al., 2022). Predota et al. (Předota et al., 2016; Biriukov et al., 2020) employed classical molecular dynamics simulations to determine the ζ potential of rutile and quartz surfaces, with the variables of temperature, salt types, and concentration, consistent with experimental results. However, the atom charge in classical MD is usually fixed, that is, the surface charge density of metal oxides is unchanged. Therefore, the classical MD ignored the dynamic change in the interface property caused by the fluids. Although the constant-potential molecular dynamic simulation (Merlet et al., 2012; Bi et al., 2020) can describe dynamic charges, the method requires too much time because the atom charges must be fitted at each step. Therefore, the MD simulation cannot describe the influence of the reservoir environment and additives on the surface charge density and ζ potential simultaneously. Therefore, there is an urgent need for a method to describe the thermodynamics of the charge regulation of rock surfaces.

In our previous work, fluid density functional theory (fluid DFT) was proven to be an efficient approach to describe the equilibrium and transport properties of ions in nanoconfinement (Lian et al., 2016; Lian et al., 2016), and chain connectivity was introduced to investigate the interface behaviors of polymer solutions with different chain lengths (Yang et al., 2020). In our recent work (Cheng et al., 2022), fluid DFT was extended to the oil recovery field to investigate the competitive adsorption between surfactants and polyelectrolytes, providing an efficient strategy for low-cost surfactant consumption. Taking the rock surface reaction into account, the behaviors of surfactants in confined conditions could be deeply understood. Therefore, the fluid DFT and surface reaction model are combined to thoroughly explore the surface charge density and ζ potential of the rock surface affected by different variables, including pH, surfactant chain length, concentration, and pore size. The structure of this work is as follows. First, the methodology, including the coarse-grained surfactant model with different chain lengths, the theoretical methods of fluid DFT, and the surface reaction model, are briefly described. Second, the fluid DFT and surface reaction model are combined to investigate the surface electrochemistry properties of the rock surface (represented by silica pores), while the effects of pH in reservoirs, the types, chain length, and concentration of surfactant, and pore size are thoroughly considered. Finally, we summarize the results, hoping to guide the industry process of CEOR.

2. Methodology

2.1. Coarse-grained model

As shown in Fig. 1, the coarse-grained model of anionic surfactant is established, and the molecules are simplified as identical-sized hard spheres (Yang et al., 2020; Wu et al., 2011; Jiang et al., 2011). In this work, the behaviors of both cationic and anionic surfactants are considered. Each surfactant consists of one charged head group and several neutral chain spheres, while the charge of the head groups is set as −1 or + 1. The mono-charged sphere is introduced as a corresponding counter ion. The charge is mainly concentrated in head groups, as the electrostatic potential is displayed in **Fig. S1**. Similar to our previous work (Cheng et al., 2022; Yang et al., 2020), each hard-sphere diameter is fixed at 0.5 nm, and the temperature is set as 298 K. Due to the coarse-grained model, molecular details and some interactions at the atomic level were neglected, such as H-bonds and chemical bonds formed between rock and surfactant, but the method is rational enough to describe the charge regulation behaviors of surfactants on the rock surface in nanoconfinements. Although real rock has a wide pore size distribution and various pore shapes (Zeng et al., 2021; Zhu et al., 2018), our work focused on a slit pore model at the nanoscale, which has been proven to capture the essential features of porous silica in electrolytes (Yang et al., 2020).

2.2. Theoretical method

2.2.1. Fluid density functional theory (Fluid DFT)

The restricted primitive model (RPM) describes the thermodynamic properties of ions in an aqueous solution, in which the ions are simplified as charged hard spheres, and the solvent environment is considered a continuum medium. In this model, the ion density distribution is defined as Eq. (1):

$$\rho_i(z) = \rho_i^0 \exp\left[-\beta V_i(z) - \beta Z_i e\psi(z) - \beta\Delta\mu_i^{ex}(z)\right] \tag{1}$$

where ρ_i^0 is the bulk ion concentration, $\beta = 1/(k_B T)$, k_B is the Boltzmann constant, T is the given temperature, Z_i is the ion valence, e is the elementary charge, and $\psi(z)$ is the electric potential. $\Delta\mu_i^{ex}(z)$ is the excess chemical potential, which is divided into four types: hard-sphere repulsion, chain connectivity, direct Coulombic energy, and electrostatic correlations; the details are described in the **Supporting Information (SI)** (Yang et al., 2020). $V_i(z)$ is the hard-sphere potential between ion spheres and the boundary wall (the silica surface in this work) and is given by

$$V_i(z) = \begin{cases} 0, d_{wall-sphere} \geq \frac{\sigma_i}{2} \\ \infty, d_{wall-sphere} < \frac{\sigma_i}{2} \end{cases} \tag{2}$$

σ_i is the hard-sphere diameter, and the hard-sphere potential between two spheres in an aqueous solution also follows this form. The electrostatic potential $\psi(z)$ of the system is obtained through the Poisson equation

$$\frac{d^2\psi(z)}{dz^2} = -\frac{\rho_i(z)}{\varepsilon_0\varepsilon_r} \tag{3}$$

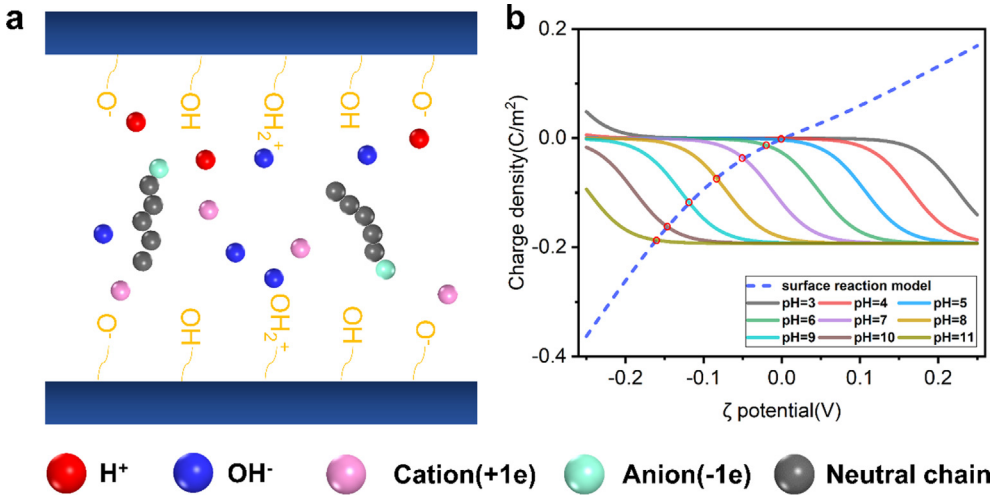

Fig. 1. (a) Schematic diagram of the surface reaction model and fluid DFT. (b) Schematic diagram of the surface potential and charge density (circled in red) determined by combining fluid DFT (dotted line) and the surface reaction model (solid lines) at different pH values. (For interpretation of the references to colour in this figure legend, the reader is referred to the web version of this article.)

in which ε_0 and ε_r are the vacuum permittivity and dielectric constant, respectively, and the boundary condition is defined as

$$\psi(0) = \psi(d) = \psi_0 \tag{4}$$

where d is the pore width. To solve Eqs. (1) and (3)-(4) numerically, an initial guess of the density profiles is carried out to obtain the electrostatic potential $\psi(z)$ and excess chemical potential $\Delta\mu_i^{ex}(z)$. Then, the new density profiles are obtained according to Eq. (1), and the process must be repeated until convergence. From the ion distributions and the electrical potential, the surface charge density could be calculated according to the overall charge neutrality condition

$$Q = -\sum_i Z_j e \int_0^{H/2} dz\rho_i(z) \tag{5}$$

2.2.2. Surface-reaction model

Silica, the main component of sandstone (Aslan et al., 2016; Alotaibi et al., 2011), is selected to represent the rock surface, and the silanol (SiOH) on the rock surface undergoes protonation/deprotonation reactions, as shown in Eqs. (6) and (7), with equilibrium constants of K_A and K_B, respectively.

$$SiOH \leftrightarrow SiO^- + H^+ \qquad K_A \tag{6}$$

$$SiOH + H^+ \leftrightarrow SiOH_2^+ \qquad K_B \tag{7}$$

where $pK_A = -\log(K_A) = 6.8$ and $pK_B = -\log(K_B) = 1.7$ (Andersen et al., 2011; Mei et al., 2016).

Due to the protonation/deprotonation reactions existing on the rock surface, the total number density of silicon components is determined by three parts, SiOH, SiO^-, and $SiOH_2^+$, as shown in Eq. (8).

$$N_{total} = N_{SiOH} + N_{SiO^-} + N_{SiOH_2^+} \tag{8}$$

Considering the protonation/deprotonation reaction equilibrium, the charge density of the rock surface is given by:

$$Q = FN_{total}\left(\frac{K_B[H^+]_s^2 - K_A}{K_A + [H^+]_s + K_B[H^+]_s^2}\right) \tag{9}$$

where F is the Faraday constant of 96,485C·mol^{-1}, N_{total} is set as 8 nm^{-2} from previous work (Lian et al., 2019), and $[H^+]_s$ is defined according to the Boltzmann equation:

$$[H^+]_s = C_0\exp\left(-\frac{z_i F\psi_0}{RT}\right) \tag{10}$$

in which C_0 is the bulk concentration of $[H^+]$ determined by the pH of the solution, ψ_0 is the surface potential, and z_i is the valence of + 1.

Based on the two methods mentioned above, the rock surface potential and charge density could be obtained by solving the intersection, as displayed in Fig. 1**(b)**. The validity of the above procedure will be demonstrated below.

3. Results and discussion

3.1. The effect of pH on the surface charge density of silica nanopores.

In the process of enhanced oil recovery, a variety of surfactants are usually applied in combination, which could simultaneously meet the requirements of emulsification, stability, and salt resistance. Therefore, both anionic and cationic surfactants are investigated in this work.

In this part, the surfactant with chain length N = 16 is selected as an example for research, and the effect of chain length will be discussed next. As shown in Fig. 2, the surface charge density of silica pores tends to be more negative as the pH increases, which is consistent with the experimental results reported for different silica samples (Murota and Saito, 2022; Salis et al., 2010). This phenomenon is attributed to the deprotonation of SiOH, in which the number of SiO^- with a negative charge increases with pH.

While its concentration and pH conditions are fixed, the absolute value of surface charge density increases with pore size, but the effect of pore size becomes negligible after reaching critical size. Therefore, the pore size effect could be found in both systems, which was relatively weak in the anionic surfactant systems compared to that in cationic surfactant systems. As shown in Fig. 2**(a)**, the surface charge density has almost no change after d is enlarged to 5 nm, which indicates that the electric double layers (EDLs) of

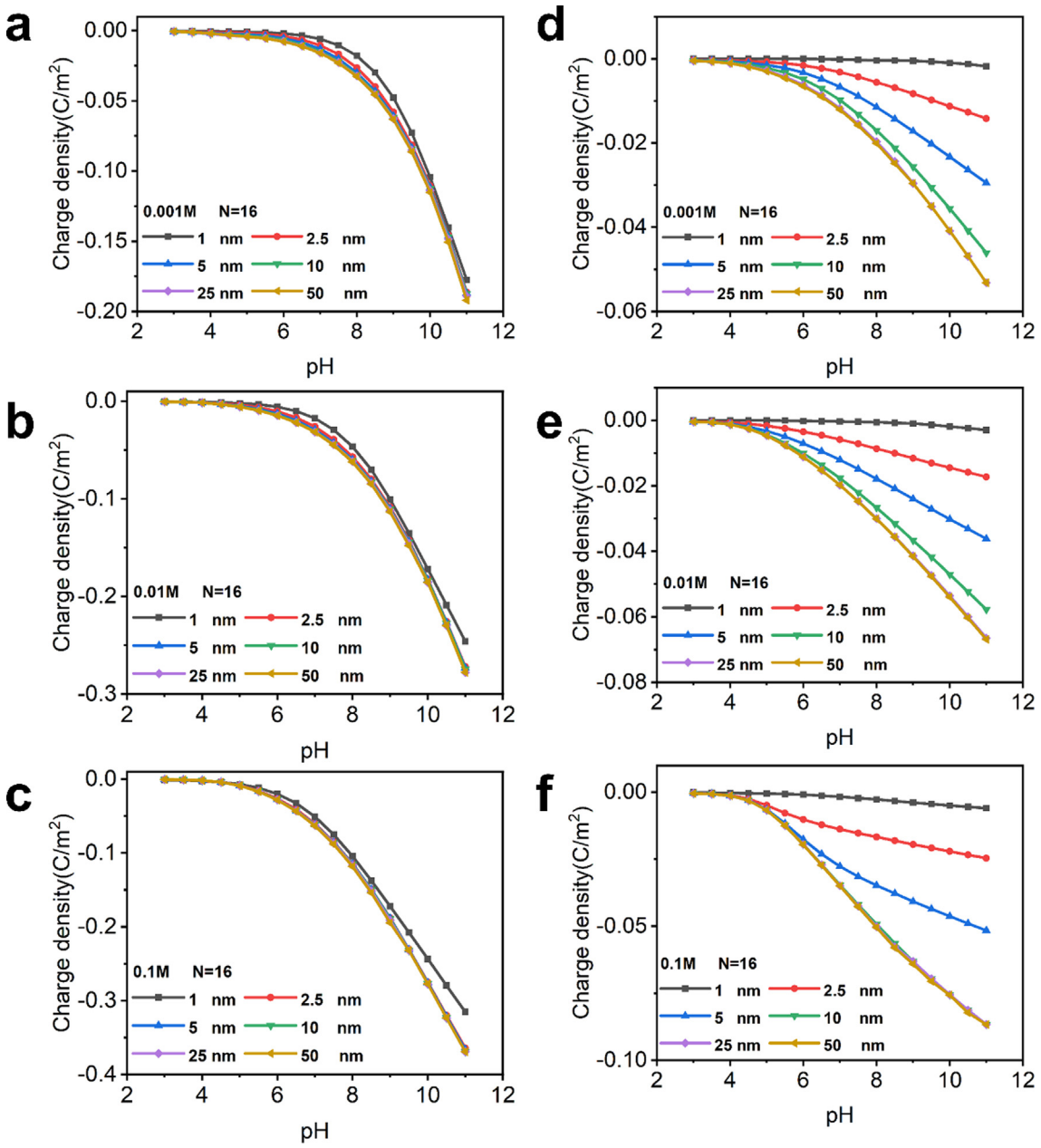

Fig. 2. The surface charge density with pH under different *d* at a concentration of *N* = 16: anionic surfactant (a) 0.001 M, (b) 0.01 M, (c) 0.1 M; cationic surfactant (d) 0.001 M, (e) 0.01 M, (f) 0.1 M.

the slit pore are independent while the pore size is large enough, so that the surface charge density approaches an asymptotic limit. After making comparisons among different concentrations, it could be found that the pore size effect is gradually reduced as the concentration increases, and the critical pore size (CPS) is 2.5 nm (0.1 M) compared to 5 nm (0.001 M) at pH = 8. The larger the surfactant concentration is, the smaller the critical pore is, which is correlated with the reduced Debye length as the surfactant concentration increases. Different from anionic surfactant systems, the CPS is relatively larger in cationic surfactant systems, the critical *d* is ~25 nm (0.001 M), and the CPS is still 10 nm when the concentration reaches 0.1 M. This phenomenon is attributed to the difference in charged head groups, and there is electrostatic repulsion between the negatively charged wall and head groups of the anionic surfactant. Therefore, the effect of charge regulation mainly depends on the counterion in anionic surfactant systems. For cationic surfactants, the positive charge is provided by head groups, and the steric effect of the neutral chain should be considered, which is much more complicated than that in anionic surfactant systems. Therefore, the CPS is relatively larger than that in cationic surfactant systems. When *N* = 2, the gap in the pore size effect is further narrowed, as shown in **Fig. S2**, which also proves the viewpoint mentioned above.

3.2. The effect of neutral chain length on the surface charge density of silica nanopores.

As mentioned in **Section 3.1**, the effect of neutral chain length should be given more attention. Therefore, the surface charge density after introducing different chain-length surfactants is investi-

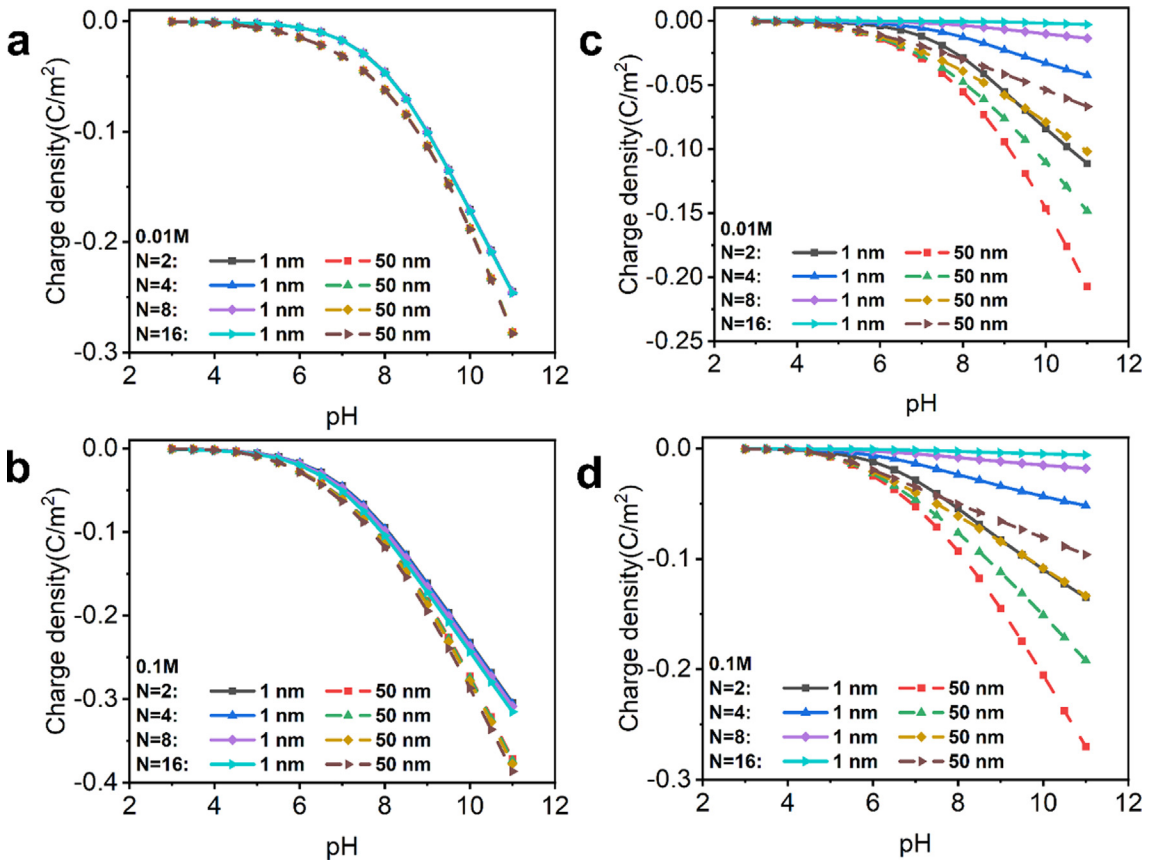

Fig. 3. The surface charge density with pH is regulated by different chain length (N = 2, 4, 8, 16) surfactants in 1 nm and 50 nm slit pores: anionic surfactant (a) 0.01 M (b) 0.1 M; cationic surfactant (c) 0.01 M (d) 0.1 M.

gated. As shown in Fig. 3**(a)**, it is found that the surface charge density has little correlation with the chain length of surfactants while the anionic surfactant concentration is relatively lower, since the concentration is low, the intermolecular interaction among surfactants is weak, and the distributions of charged head groups and counter ions are similar in both systems. In Fig. 3**(b)**, the effect of chain length gradually emerges as the anionic surfactant concentration increases, but the difference is still not significant. For cationic surfactants, it is obvious that the chain length plays a vital role in charge regulation because the positively charged head groups are connected with the neutral chain length. The shorter the neutral chain length is, the easier it is for the surfactant to enter the pores to interact with the negative pore wall. Therefore, the neutral chain length effect cannot be neglected in cationic surfactant systems.

To demonstrate the effect of chain length, we directly obtain the density distribution of different species at the interface based on fluid DFT, as shown in Figs. 4 and 5. In this section, we use pH = 8 as an example and explore the density distribution of charged head groups, neutral side chains, and counter ions along the z-direction of the nanopore. The ζ potential at this pH is obtained as the initial parameter based on combining the fluid DFT and surface reaction model.

As the anionic surfactant is introduced, it is found that the density profiles of charged species, including head groups and counter ions, are similar in these systems with low concentrations, as mentioned above. The concentration of head groups near the pore wall is negligible compared to that of counter ions because of the repulsion between the pore wall and head groups, in which the charge regulation behaviors are similar to those of the simple salt. When the surfactant concentration increases, the counter ions are more dominantly distributed at the interface compared to head groups, and the density of counter ions at the interface follows $N = 16 > N = 8 > N = 4 > N = 2$, as shown in Fig. 4**(b)-(c)**. The longer the chain length is, the more counter ions there are at the interface. To ensure the local electrical neutrality of the interface induced by counter ions, the rock surface in $N = 16$ systems should behave with more negative charges; therefore, the surface charge density of $N = 16$ is the most negative. By comparing the density profiles between head groups and neutral chain species, it could be found that the neutral chain tends to interact with the surface. Since the interface is negatively charged, the head groups are repulsed by the electrostatic effect. The neutral chain is close to the surface through the nonelectrostatic effect, which has been proven by MD simulation (Zhong et al., 2013; Tummala et al., 2011). Moreover, there are also interactions among neutral chains, so it is relatively difficult for the head groups of the $N = 16$ surfactant to access the surface because of the steric hindrance formed by the neutral chain.

In cationic surfactant systems, the difference in the density distribution of head groups is significantly contrary to anionic surfactants, and the effect of counter ions is neglected. Because the short surfactant could enter the pore with a low energy barrier, the density distribution of head groups follows $N = 2 > N = 4 > N = 8 > N = 16$. Therefore, the $N = 2$ systems show a more negative surface charge to maintain the local electrical neutrality, consistent with Fig. 3**(c)-(d)**. Different from the anionic surfactant systems, the head groups are closer to the pore wall than the neutral chains

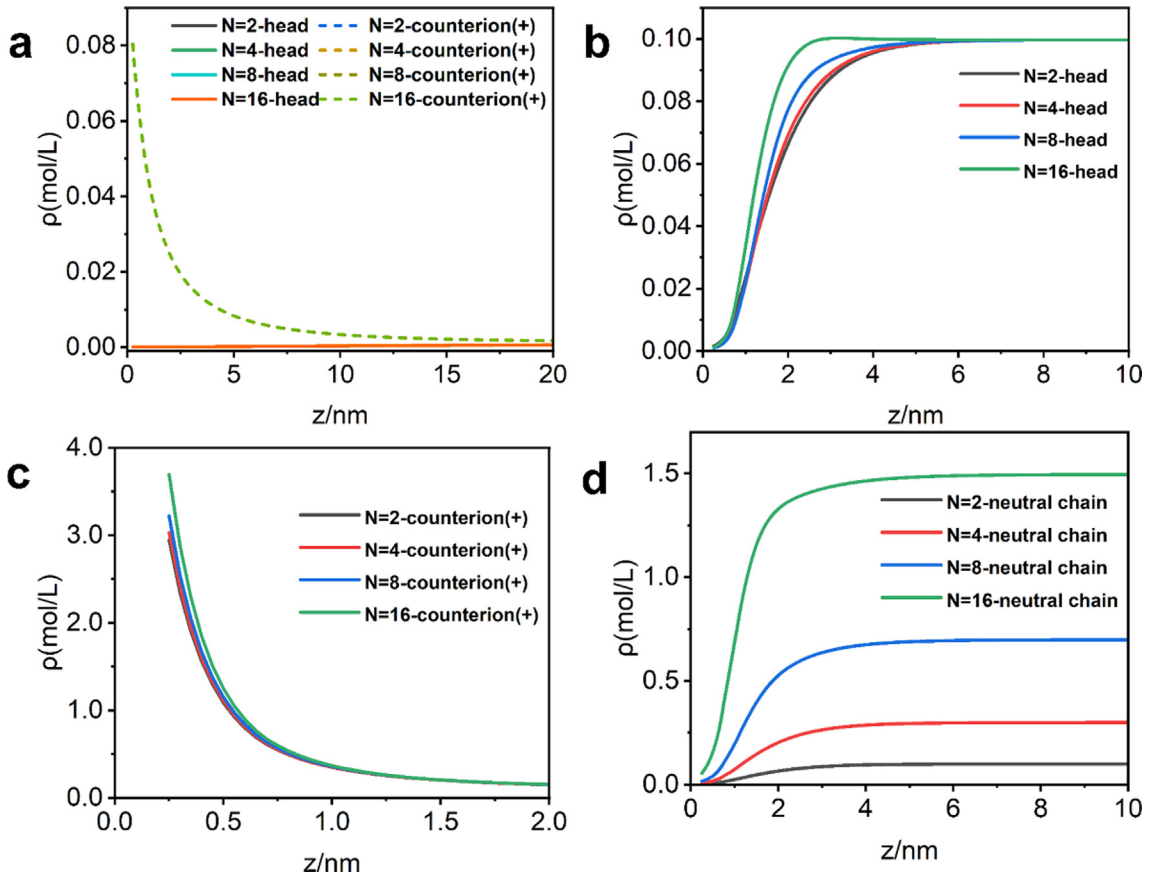

Fig. 4. (a) Density profiles of head groups and counter ions of anionic surfactants (N = 2–16) under 0.001 M; Density profiles of (b) head (c) counter ions and (d) neutral chains of surfactant (N = 2–16) under 0.1 M. (d = 50 nm is fixed).

by comparing Fig. 5**(b)-(c)**; therefore, the anionic surfactant may be adsorbed on the negative pore wall by electrostatic attraction during the EOR process.

3.3. The nanoconfinement behavior in silica nanopores.

Although the density distributions of each species at 50 nm have been investigated, the confinement effect of nanopores at different scales is still unclear due to their complex pore structures. Especially at the subnanoscale, fluids are induced to exhibit different properties deviating from the bulk phase (Nazari et al., 2020). Therefore, exploring the phase behaviors of each species under other pores is important.

As shown in Fig. 6**(a)**, there are almost no anionic surfactants in the 1 nm slit, although the concentration of the bulk phase is 0.1 M, which is easily understood because the entry barrier is difficult to overcome due to the electrostatic repulsion effect between the negatively charged rock surface and head groups. As the pore size increases, some surfactant molecules enter the slit. The surfactant concentration is similar to that of the bulk, while d is larger than 5.0 nm. As shown in Fig. 6**(c)-(d)**, the bulk concentrations of the head groups and neutral chains in the slit are almost identical, with a concentration of 0.1 M and 1.5 M, respectively.

As shown in Fig. 7, contrary to the anionic surfactant, the cationic surfactant could enter the 1 nm pore, but the concentration of head groups in pores is 0.02 mol/L, different from the bulk phase. With increasing pore size, the surfactant concentration far from the pore wall gradually approaches the bulk phase. When d = 50 nm, the bulk concentration of head groups and neutral chains in the pore is 0.1 M, and 1.5 M, respectively, in which the pore is similar to the open space, and the nanoconfinement effect may be neglected. These results also proved the rationality of the pore size range.

3.4. The effect of surfactant concentration on surface properties of silica nanopores.

As shown in Fig. 8, the effect of the surfactant concentration on the surface charge density is investigated. Taking the N = 16 anionic surfactant and d = 1 nm as an example, the absolute value of the surface charge density decreases with decreasing surfactant concentration, which is consistent with our previous work (Yang et al., 2020). For example, when pH = 8, the surface charge density is $-0.1043 C/m^2$ at 0.1 M, compared to $-0.018 C/m^2$ at 0.001 M. At relatively higher concentrations, the counter ions more easily participate in surface charge regulation, while the confined space is unchanged. As shown in Fig. 8**(c)-(d)**, the correlation between cationic surfactant concentration and surface charge density shows similar trends with the anionic surfactant, but the surface charge density in anionic surfactant systems is more negative than that in cationic surfactant systems, which is attributed to the energy barrier difference between positively charged mono counter ions and the head groups. As described in Figs. 4**(c)** and 5**(b)**, the density of anionic surfactants' counter ions is larger than that of cationic surfactants' head groups; therefore, the surface charge density is more negative in anionic surfactant systems.

Taking the surface reaction model into account as Eq. (9), the factor that directly determines surface charge density is the proton

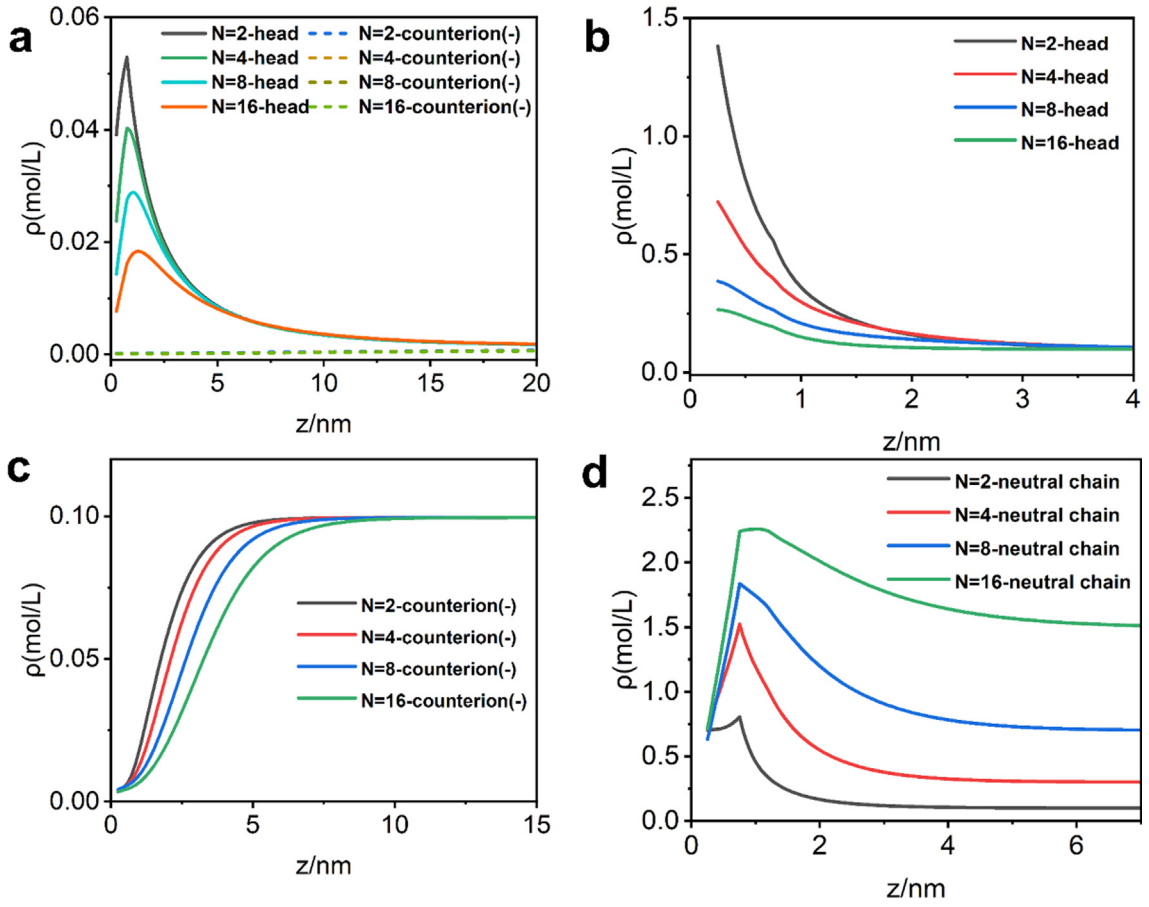

Fig. 5. (a) Density profiles of head groups and counter ions of cationic surfactants (N = 2–16) under 0.001 M; Density profiles of (b) head (c) counter ions and (d) neutral chains of surfactant (N = 2–16) under 0.1 M. (d = 50 nm is fixed).

concentration, $[H^+]$. Therefore, surfactants with different concentrations induce variable behaviors of surface charge density by affecting the surface proton concentration. Fig. 9**(a)** shows that $[H^+]$ decreases with the surfactant concentration, which promotes the deprotonation reaction of silica pores considering reaction equilibrium so that the negative species of SiO^- increase, resulting in more negative surface charge density. It is obviously indicated that the proton concentration is significantly affected by pore size under low surfactant concentrations, and the proton concentration is reduced from $7.05 \times 10^{-6}M$ to $3.78 \times 10^{-6}M$ when d changes from 1 nm to 50 nm with a surfactant concentration of 0.001 M. When the surfactant is 0.1 M, the proton concentration shows less change after d exceeds 2.5 nm, which is consistent with the CPS. The correlation between the surface proton concentration and cationic surfactant concentration is similar to that of anionic surfactant systems, as shown in **Fig. S3**.

Furthermore, the ζ potential is the factor that directly affects $[H^+]$ under a fixed pH according to Eq. (10). Therefore, we investigate the effect of the surfactant concentration on the ζ potential. As shown in Fig. 9**(b)**, the absolute value of the ζ potential decreases as the concentration of the surfactant increases. However, the absolute value of the surface charge density becomes higher, as mentioned above. According to previous work (Gilbert and Ehrenstein, 1969; Mozhayeva and Naumov, 1970; McLaughlin et al., 1971; McLaughlin et al., 1981), the ions in an aqueous solution could affect the ζ potential not only by binding to the counter charge on the surface but also by exerting a screening effect. Therefore, we considered that this phenomenon might be related to the charge screening effect under different surfactant concentrations. It is well known that the Debye length, $\lambda_D = \sqrt{\varepsilon_0 \varepsilon_r RT / \sum_i^2 F^2 z_i^2 c_{i0}}$, is significantly dependent on the surfactant concentration in aqueous solution (Kato et al., 2018). The λ_D are 9.61 nm, 3.04 nm, and 0.96 nm, respectively, while the surfactant ranges from 0.001 M, 0.01 M to 0.1 M. The Debye length differed approximately tenfold, which indicates that the ions in the much smaller area near the rock surface have effects on the surface, although the ion concentration increases; thus, the ζ potential becomes less negative. Since both surface charge density and ζ potential are affected by solution conditions, the surface charge density is positively correlated with ζ potential at a given concentration. When the concentration of ions in the system changes, the lower ion concentration results in less electrostatic shielding, causing a larger surface potential (Ong et al., 2020). Similar to our work, Predota et al. (Předota et al., 2016; Biriukov et al., 2020) carried out molecular dynamics simulations to investigate the effect of inorganic salt concentration on the ζ potential of SiO_2 (1 0 1), in which they found that the ζ potential tended to be more negative as the NaCl concentration decreased, which is consistent with the experimental results obtained by Leroy et al. (Leroy et al., 2013). Moreover, Buckley et al. (Buckley et al., 1989) also proposed that the zeta potential of the glass/oil interface was reduced as the Na^+ concentration increased. Therefore, the validity of our model could be proven

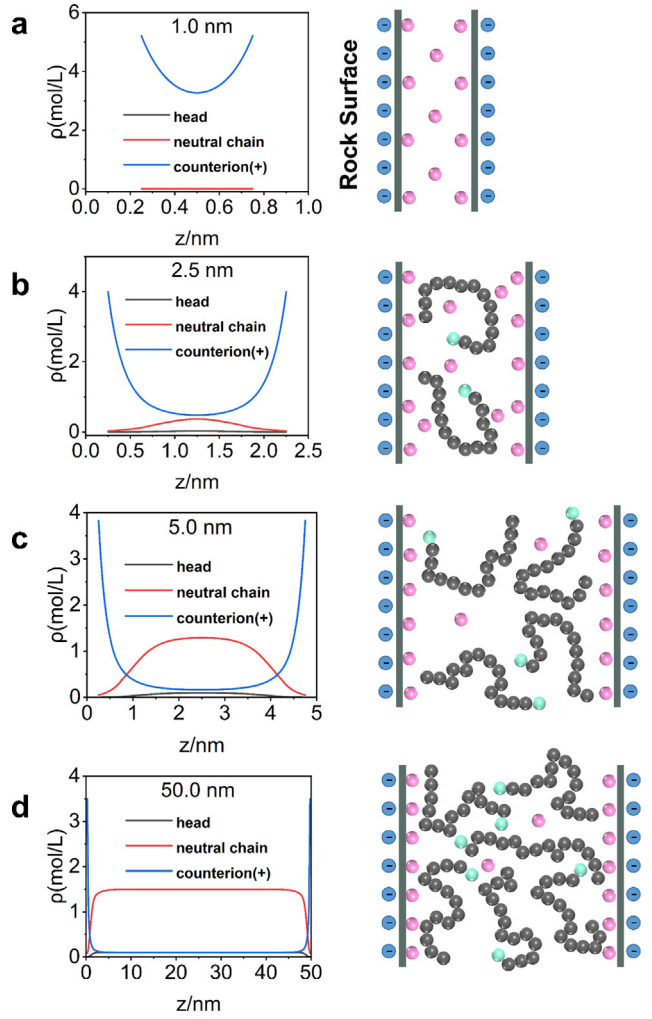

Fig. 6. Density profiles of head groups (black) and neutral chain groups (red) of $N = 16$ anionic surfactants and counter ions (blue) in rock pores at 0.1 M. 1.0 nm, (b) 2.5 nm, (c) 5.0 nm and (d) 50.0 nm. (The colored beads representing different species are the same in Fig. 1.) (For interpretation of the references to colour in this figure legend, the reader is referred to the web version of this article.)

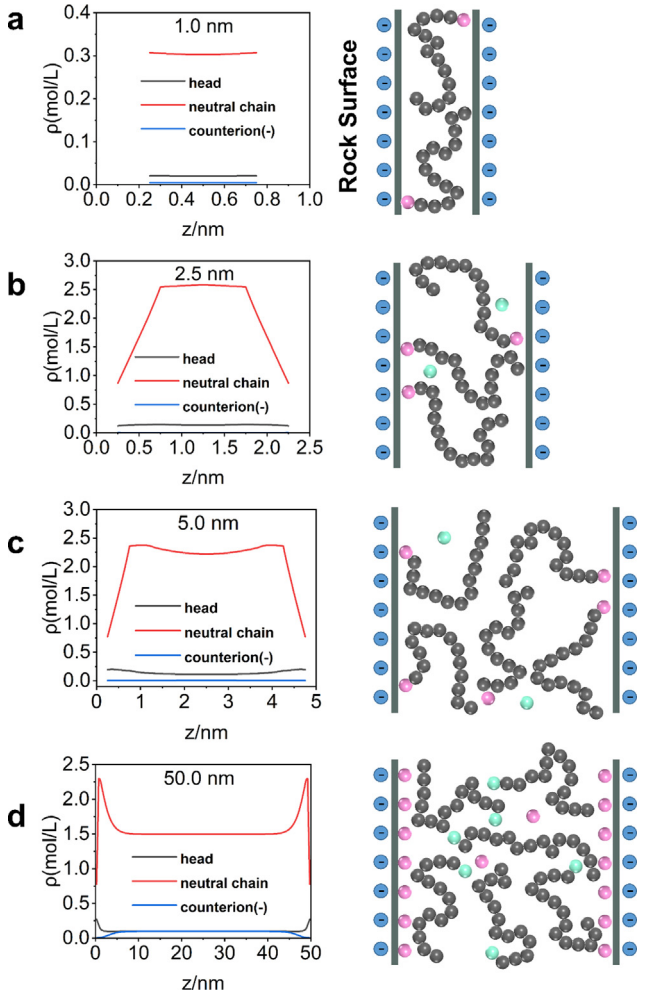

Fig. 7. Density profiles of head groups (black) and neutral chain groups (red) of $N = 16$ cationic surfactants and counter ions (blue) in rock pores at 0.1 M. (a) 1.0 nm, (b) 2.5 nm, (c) 5.0 nm and (d) 50.0 nm. (The colored beads representing different species are the same in Fig. 1.) (For interpretation of the references to colour in this figure legend, the reader is referred to the web version of this article.)

by the experiment and MD simulation. Meanwhile, our method has more advantages than MD, especially in computational efficiency, as shown in **Table S1**.

To further reveal the effect of the surfactant concentration on the surface electrical properties, a series of concentration gradients are investigated, in which d is fixed at 50 nm, so that the size effect could be negligible. The normalized ζ potential and Debye length are shown in Fig. 10, with 0.001 M as a reference. The correlation between the concentration and ζ potential shows a similar trend as that between the concentration and Debye length, which validates the conclusion mentioned above that increasing the surfactant concentration causes a less negative ζ potential through electrostatic screening. Moreover, it should be noted that the surfactant concentration has little effect when the concentration is more than 0.04 M, especially compared to the concentration ranging from 0.001 M to 0.01 M. Therefore, the charge regulation performance of the surfactant is not linearly correlated with its concentration, and there is an upper regulation limit. Taking 0.1 M and 0.4 M, for example, when the anionic surfactant concentration is increased by three times, the ζ potential decreases by only 6%. As shown in Fig. 10, the change in the normalized ζ potential in cationic surfactant systems is relatively smaller than that in anionic surfactant systems because there is an interaction among the neutral chains of the cationic surfactant, and the charge regulation behavior is different from the effect of mono ions in anionic surfactant systems. Furthermore, the correlation between concentration and normalized ζ potential provides an effective theoretical prediction method for balancing the cost and charge regulation performance of surfactants.

4. Conclusion

In this work, the method of combining fluid DFT and a surface reaction model is used to investigate the effect of both anionic and cationic surfactants' chain length, concentration, and pore size on the surface charge density and ζ potential of silica nanopores, which are listed as follows.

1. The surface charge density becomes more negative with increasing pH due to the deprotonation reaction, causing the number of negative species to increase. The pore size effect

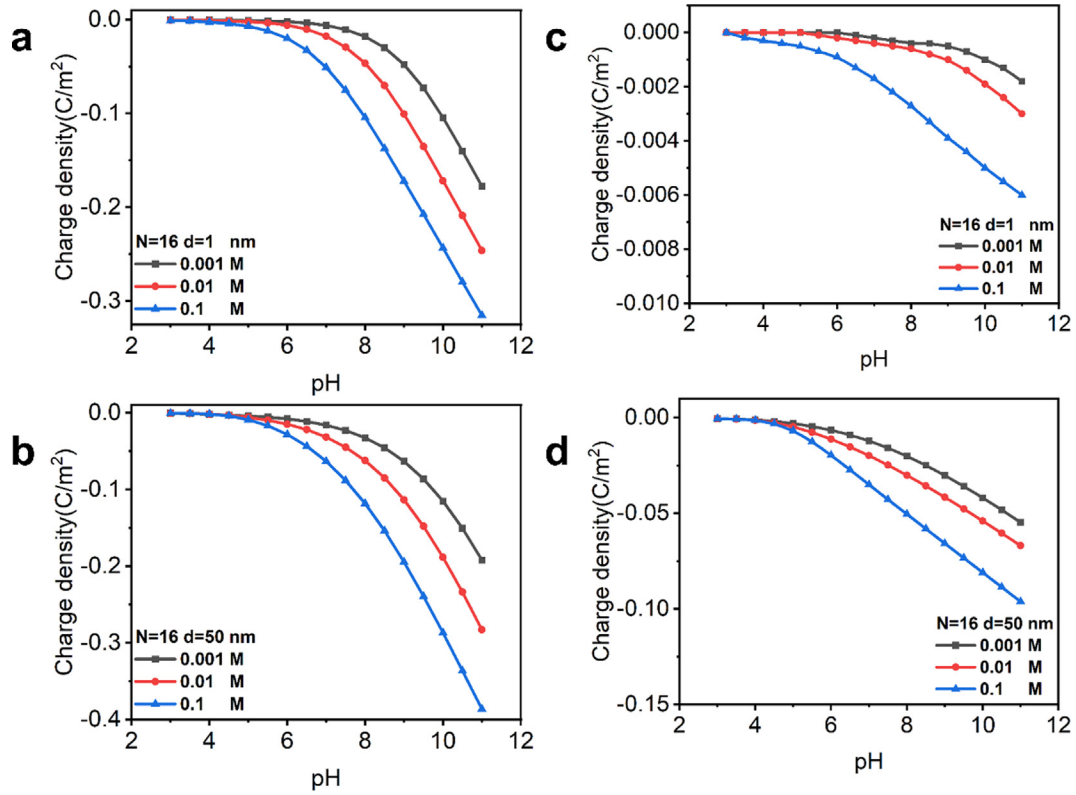

Fig. 8. The surface charge density with pH as the N = 16 surfactant concentration changed. (a) d = 1 nm; (b) d = 50 nm.

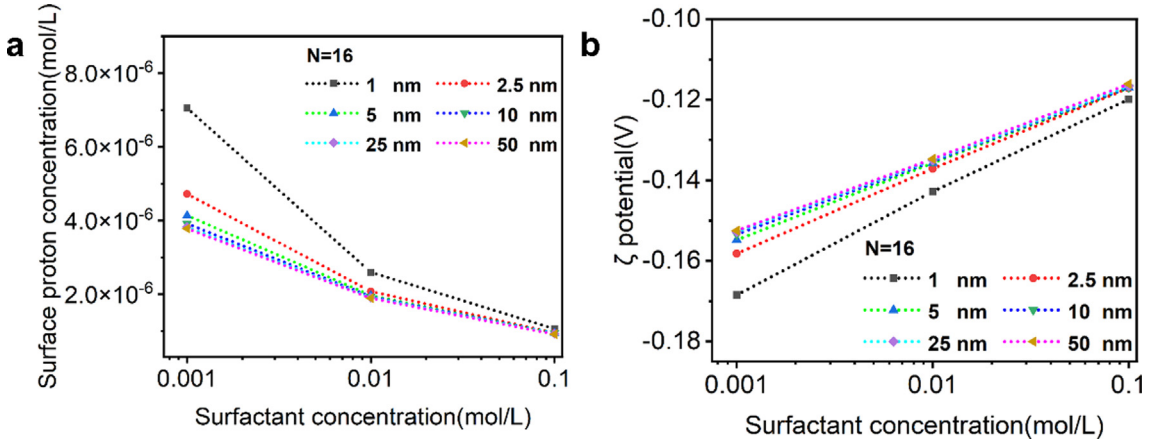

Fig. 9. (a) Surface proton concentration, (b) ζ potential with N = 16 anionic surfactant concentration.

plays an important role in surface charge density, but the surface charge density approaches an asymptotic limit after exceeding CPS, in which the EDLs are negligible compared to pore size, and the pore size effect is less significant at high surfactant concentration and pH conditions.

2. The chain length effect is significant in cationic surfactant systems compared to anionic surfactants, and the effect of anionic surfactants is similar to that of simple salts due to the electrostatic repulsion between the pore wall and head groups. In cationic surfactant systems, the chain length causes a difference in steric hindrance to enter the pore. The shorter the neutral chain length is, the more negative the surface charge density.
3. The surface charge density becomes more negative as the surfactant concentration increases, but the ζ potential tends to be less negative, which could be attributed to the strong electrostatic screening. The normalized ζ potential and Debye length have been calculated to exhibit the correlation between the charge regulation performance and concentration of the surfactant, and the surface properties tend to be stable as the surfactant concentration increases.

The results are validated by previous MD simulations and experimental results, which proved the efficiency and accuracy of this method. This work demonstrates that the process of combin-

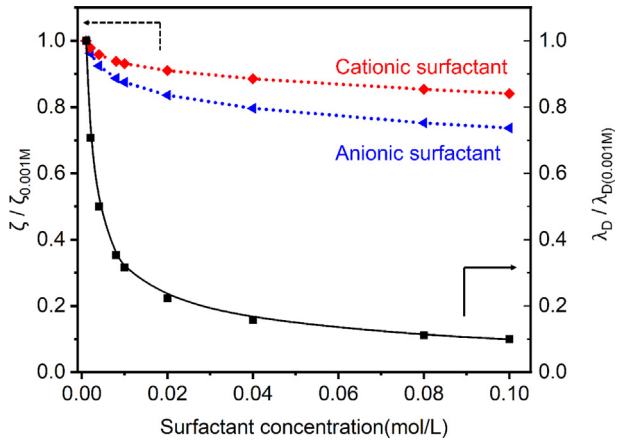

Fig. 10. The normalized ζ potential (solid black line) and Debye length (blue dotted line) with different surfactant concentrations. (For interpretation of the references to colour in this figure legend, the reader is referred to the web version of this article.)

ing fluid DFT and a surface reaction model could properly describe the surface electrochemical properties of silica pores under different reservoir conditions, hoping to guide the EOR process.

CRediT authorship contribution statement

Jipeng Xu: Methodology, Formal analysis, Writing – original draft. **Jin Cheng:** Formal analysis, Writing – original draft. **Jie Yang:** Writing – review & editing. **Haolan Tao:** Writing – review & editing. **Sijie Wang:** Writing – review & editing. **Wenjie Lv:** Writing – review & editing. **Ke Ma:** Writing – review & editing. **Cheng Lian:** Conceptualization, Resources, Funding acquisition, Writing – review & editing, Supervision. **Honglai Liu:** Resources.

Data availability

Data will be made available on request.

Declaration of Competing Interest

The authors declare that they have no known competing financial interests or personal relationships that could have appeared to influence the work reported in this paper.

Acknowledgments

This work was sponsored by the National Key R&D Program of China (No. 2019YFC1906702), the State Key Laboratory of Clean Energy Utilization (Open Fund Project No. ZJUCEU2021005), the Fundamental Research Funds for the Central Universities (2022ZFJH004), the National Natural Science Foundation of China (No. 22278127) and the Shanghai Rising-Star Program (No. 21QA1401900).

Appendix A. Supplementary material

Supplementary data to this article can be found online at https://doi.org/10.1016/j.ces.2023.118718.

References

Alotaibi, M.B.B., Nasralla, R.A.A., Nasr-El-Din, H.A.A., 2011. Wettability studies using low-salinity water in sandstone reservoirs. SPE Reserv. Eval. Eng. 14 (06), 713–725.
Alotaibi, M.B., Nasr-El-Din, H.A., 2011. Electrokinetics of limestone particles and crude-oil droplets in saline solutions. SPE Reserv. Eval. Eng. 14 (05), 604–611.
Alroudhan, A., Vinogradov, J., Jackson, M.D., 2016. Zeta potential of intact natural limestone: impact of potential-determining ions Ca, Mg and SO4. Colloids Surf. A Physicochem. Eng. Asp 493, 83–98.
Aminian, A., ZareNezhad, B., 2019. Oil-detachment from the calcium carbonate surfaces via the actions of surfactant, nanoparticle and low salinity brine: an insight from molecular dynamic simulation. Chem. Eng. Sci. 202, 373–382.
Amiri, S., Gandomkar, A., 2019. Influence of electrical surface charges on thermodynamics of wettability during low salinity water flooding on limestone reservoirs. J. Mol. Liq. 277, 132–141.
Andersen, M.B., Frey, J., Pennathur, S., Bruus, H., 2011. Surface-dependent chemical equilibrium constants and capacitances for bare and 3-cyanopropyldimethylchlorosilane coated silica nanochannels. J. Colloid Interface Sci. 353 (1), 301–310.
Aslan, S., Fathi Najafabadi, N., Firoozabadi, A., 2016. Non-monotonicity of the contact angle from NaCl and MgCl2 concentrations in two petroleum fluids on atomistically smooth surfaces. Energy Fuel 30 (4), 2858–2864.
Bi, S., Banda, H., Chen, M., Niu, L., Chen, M., Wu, T., Wang, J., Wang, R., Feng, J., Chen, T., Dincă, M., Kornyshev, A.A., Feng, G., 2020. Molecular understanding of charge storage and charging dynamics in supercapacitors with MOF electrodes and ionic liquid electrolytes. Nat. Mater. 19 (5), 552–558.
Biriukov, D., Fibich, P., Předota, M., 2020. Zeta potential determination from molecular simulations. J. Phys. Chem. C 124 (5), 3159–3170.
Brkljača, Z., Namjesnik, D., Lützenkirchen, J., Předota, M., Preočanin, T., 2018. Quartz/aqueous electrolyte solution interface: molecular dynamic simulation and interfacial potential measurements. J. Phys. Chem. C 122 (42), 24025–24036.
Buckley, J.S., Takamura, K., Morrow, N.R., 1989. Influence of electrical surface charges on the wetting properties of crude oils. SPE Reserv. Eng. 4 (03), 332–340.
Cao, Y., Malekshah, R.E., Heidari, Z., Pelalak, R., Marjani, A., Shirazian, S., 2021. Molecular dynamic simulations and quantum chemical calculations of adsorption process using amino-functionalized silica. J. Mol. Liq. 330, 115544.
Cheng, J., Xu, J., Yang, J., Lv, W., Lian, C., Liu, H., 2022. Enhanced oil recovery by sacrificing polyelectrolyte to reduce surfactant adsorption: a classical density functional theory study. Chem. Eng. Sci. 117957.
Chowdhury, S., Shrivastava, S., Kakati, A., Sangwai, J.S., 2022. Comprehensive review on the role of surfactants in the chemical enhanced oil recovery process. Ind. Eng. Chem. Res. 61 (1), 21–64.
El Haouti, R., Ouachtak, H., El Guerdaoui, A., Amedlous, A., Amaterz, E., Haounati, R., Addi, A.A., Akbal, F., El Alem, N., Taha, M.L., 2019. Cationic dyes adsorption by Na-Montmorillonite Nano Clay: experimental study combined with a theoretical investigation using DFT-based descriptors and molecular dynamics simulations. J. Mol. Liq. 290, 111139.
Gandomkar, A., Rahimpour, M.R., 2015. Investigation of low-salinity waterflooding in secondary and tertiary enhanced oil recovery in limestone reservoirs. Energy Fuel 29 (12), 7781–7792.
Gandomkar, A., Ghorbani Sheykhneshin, M., Nasriani, H.R., Yazdkhasti, P., Safavi, M. S., 2022. Enhanced oil recovery through synergy of the interfacial mechanisms by low salinity water alternating carbon dioxide injection. Chem. Eng. Res. Des. 188, 462–472.
Gilbert, D.L., Ehrenstein, G., 1969. Effect of divalent cations on potassium conductance of squid axons: determination of surface charge. Biophys. J . 9 (3), 447–463.
Jackson, M.D., Al-Mahrouqi, D., Vinogradov, J., 2016. Zeta potential in oil-water-carbonate systems and its impact on oil recovery during controlled salinity water-flooding. Sci. Rep. 6 (1), 37363.
Jiang, D.-E., Meng, D., Wu, J., 2011. Density functional theory for differential capacitance of planar electric double layers in ionic liquids. Chem. Phys. Lett. 504 (4), 153–158.
Kamal, M.S., Hussein, I.A., Sultan, A.S., 2017. Review on surfactant flooding: phase behavior, retention, IFT, and field applications. Energy Fuel 31 (8), 7701–7720.
Kato, H., Nakamura, A., Banno, H., Shimizu, M., 2018. Separation of different-sized silica nanoparticles using asymmetric flow field-flow fractionation by control of the Debye length of the particles with the addition of electrolyte molecules. Colloids Surf. A Physicochem. Eng. Asp 538, 678–685.
Koleini, M.M., Mehraban, M.F., Ayatollahi, S., 2018. Effects of low salinity water on calcite/brine interface: a molecular dynamics simulation study. Colloids Surf. A Physicochem. Eng. Asp 537, 61–68.
Leroy, P., Devau, N., Revil, A., Bizi, M., 2013. Influence of surface conductivity on the apparent zeta potential of amorphous silica nanoparticles. J. Colloid Interface Sci. 410, 81–93.
Lian, C., Liu, K., Van Aken, K.L., Gogotsi, Y., Wesolowski, D.J., Liu, H.L., Jiang, D.E., Wu, J.Z., 2016. Enhancing the capacitive performance of electric double-layer capacitors with ionic liquid mixtures. ACS Energy Lett. 1 (1), 21–26.
Lian, C., Jiang, D.-E., Liu, H., Wu, J., 2016. A generic model for electric double layers in porous electrodes. J. Phys. Chem. C 120 (16), 8704–8710.
Lian, C., Kong, X., Liu, H., Wu, J., 2019. Flow effects on silicate dissolution and ion transport at an aqueous interface. PCCP 21 (13), 6970–6975.
McLaughlin, S., Mulrine, N., Gresalfi, T., Vaio, G., McLaughlin, A., 1981. Adsorption of divalent cations to bilayer membranes containing phosphatidylserine. J. Gen. Physiol. 77 (4), 445–473.
McLaughlin, S.G.A., Szabo, G., Eisenman, G., 1971. Divalent ions and the surface potential of charged phospholipid membranes. J. Gen. Physiol. 58 (6), 667–687.

Mei, L., Chou, T.-H., Cheng, Y.-S., Huang, M.-J., Yeh, L.-H., Qian, S., 2016. Electrophoresis of pH-regulated nanoparticles: impact of the Stern layer. PCCP 18 (15), 9927–9934.
Merlet, C., Rotenberg, B., Madden, P.A., Taberna, P.-L., Simon, P., Gogotsi, Y., Salanne, M., 2012. On the molecular origin of supercapacitance in nanoporous carbon electrodes. Nat. Mater. 11 (4), 306–310.
Mozhayeva, G.N., Naumov, A.P., 1970. Effect of surface charge on the steady-state potassium conductance of nodal membrane. Nature 228 (5267), 164–165.
Murota, K., Saito, T., 2022. Pore size effects on surface charges and interfacial electrostatics of mesoporous silicas. PCCP 24 (30), 18073–18082.
Nasralla, R.A., Bataweel, M.A., Nasr-El-Din, H.A., 2013. Investigation of wettability alteration and oil-recovery improvement by low-salinity water in sandstone rock. J. Can. Pet. Technol. 52 (02), 144–154.
Nazari, M., Davoodabadi, A., Huang, D., Luo, T., Ghasemi, H., 2020. Transport phenomena in nano/molecular confinements. ACS Nano 14 (12), 16348–16391.
Ong, G.M.C., Gallegos, A., Wu, J., 2020. Modeling surface charge regulation of colloidal particles in aqueous solutions. Langmuir 36 (40), 11918–11928.
Předota, M., Machesky, M.L., Wesolowski, D.J., 2016. Molecular origins of the zeta potential. Langmuir 32 (40), 10189–10198.
Ritt, C.L., de Souza, J.P., Barsukov, M.G., Yosinski, S., Bazant, M.Z., Reed, M.A., Elimelech, M., 2022. Thermodynamics of charge regulation during ion transport through silica nanochannels. ACS Nano.
Salis, A., Parsons, D.F., Boström, M., Medda, L., Barse, B., Ninham, B.W., Monduzzi, M., 2010. Ion specific surface charge density of SBA-15 mesoporous silica. Langmuir 26 (4), 2484–2490.
Tummala, N.R., Shi, L., Striolo, A., 2011. Molecular dynamics simulations of surfactants at the silica–water interface: anionic vs nonionic headgroups. J. Colloid Interface Sci. 362 (1), 135–143.
Wu, J., Jiang, T., Jiang, D.-E., Jin, Z., Henderson, D., 2011. A classical density functional theory for interfacial layering of ionic liquids. Soft Matter 7 (23), 11222–11231.
Xu, J., Wang, N., Xue, S., Zhang, H., Zhang, J., Xia, S., Han, Y., 2022. Insights into the mechanism during viscosity reduction process of heavy oil through molecule simulation. Fuel 310, 122270.
Xu, J.P., Xue, S., Zhang, J.L., Han, Y., Xia, S.Q., 2021. Molecular design of the amphiphilic polymer as a viscosity reducer for heavy crude oil: from mesoscopic to atomic scale. Energy Fuel 35 (2), 1152–1164.
Yang, J., Su, H., Lian, C., Shang, Y., Liu, H., Wu, J., 2020. Understanding surface charge regulation in silica nanopores. PCCP 22 (27), 15373–15380.
Yang, J., Lian, C., Liu, H., 2020. Chain length matters: Structural transition and capacitance of room temperature ionic liquids in nanoporous electrodes. Chem. Eng. Sci. 227, 115927.
Zeng, S., Li, H., Zhang, N., Sun, B., Li, J., Liu, Y., 2021. Full-scale pore size distribution features of uranium-bearing sandstone in the northwest of Xinjiang, China. Royal Soc. Open Sci. 8, (5) 202036.
Zhong, J., Wang, P., Zhang, Y., Yan, Y., Hu, S., Zhang, J., 2013. Adsorption mechanism of oil components on water-wet mineral surface: a molecular dynamics simulation study. Energy 59, 295–300.
Zhu, H., Ju, Y., Qi, Y., Huang, C., Zhang, L., 2018. Impact of tectonism on pore type and pore structure evolution in organic-rich shale: Implications for gas storage and migration pathways in naturally deformed rocks. Fuel 228, 272–289.